



Effect of eggshell powder on the microstructural and thermal behavior of Al7075/waste eggshell surface composites produced by solid-state friction stir processing developed for potential thermal applications

Ashish Kumar Srivastava¹ · Akash Nag² · Suryank Dwivedi³ · Amit Rai Dixit³ · Sergej Hloch^{2,4} 

Received: 31 January 2023 / Accepted: 14 May 2023 / Published online: 25 May 2023
© The Author(s) 2023

Abstract

Lightweight composite materials for potential thermal applications are the contemporary demand for manufacturing and aircraft industries where the possibility to improve and tailor the desired properties is based on the application. Carbonized eggshell powder is a solid lubricant with absorbent capability and has proven as a reinforcement for metallic base composites. In the present work, an attempt is made to investigate the effect of carbonized chicken eggshell powder (3 to 9% by weight) on the microstructural and thermal properties of Al7075 alloy processed by solid-state friction stir processing. An infrared thermography and three K-type thermocouples equipped with the base plate at three equal distances are used to measure the temperature with respect to time. The comparative study of microstructure and grain structure analysis has been done by light microscopy, scanning electron microscopy, and electron backscattered diffraction methods. The findings explored the dynamic recrystallization and grain recovery with a reduced grain size of 6.2 to 10.3 μm at a varying percentage of eggshell powder (3 to 9%) in the stir zone. The thermal conductivity and coefficient of thermal expansion (CTE) were measured for the temperature range of 50 to 400 $^{\circ}\text{C}$. In addition to it, differential thermal analysis (DTA), thermo-gravimetric analysis (TGA), and derivative thermo-gravimetric analysis (DTG) are conducted for the temperature range of 25 to 900 $^{\circ}\text{C}$ to discuss the endothermic, exothermic nature, and degradation characteristics. The result revealed the decreasing trend of thermal conductivity, and CTE values were found in the range of 97 to 53 W/mK and 26.6 to $24 \times 10^{-6} \text{ K}^{-1}$ (heating cycle), 27.2 to $23.8 \times 10^{-6} \text{ K}^{-1}$ (cooling cycle), respectively. Furthermore, the higher and lower thermal conductivity of 108 W/mK and 62 W/mK is observed at higher and lower terminal voltages, 250 V and 100 V, respectively. The DTA, TGA, and DTG curves explored the maximum weight loss, which varies up to 5.25% with exothermic peaks and decomposition steps for each surface composite.

Keywords Al7075 alloy · Eggshell waste · Friction stir processing · Infrared thermography · Thermal conductivity · CTE

Abbreviations

MMC Metal matrix composite
FSP Friction stir processing

ESP Eggshell powder
TC Thermal conductivity
CTE Coefficient of thermal expansion
DTA Differential thermal analysis,
TGA Thermo-gravimetric analysis
DTG Derivative thermo-gravimetric analysis

✉ Sergej Hloch
sergej.hloch@tuke.sk

¹ G L Bajaj Institute of Technology and Management, Greater Noida, UP 201308, India

² Faculty of Mechanical Engineering, VŠB - Technical University of Ostrava, Poruba, Ostrava 708 00, Czech Republic

³ Indian Institute of Technology (ISM), Dhanbad, Jharkhand 826004, India

⁴ Faculty of Manufacturing Technologies, Technical University of Košice, Prešov, Slovakia

1 Introduction

Many electronic and automobile industries face challenges with sustainable materials working in heating and cooling environments with the desired tailored properties [1]. These challenges encouraged the development of novel lightweight composite materials with a high strength-to-weight ratio, which can improve results at any working temperature.

The problems related to the high-temperature application in electronic industries, like integrated circuits, chips, and electronic pads, require proper heat dissipation while working [2]. Similarly, in automobile and aircraft components, the engine components are subjected to high temperatures and require continuous lubrication [3]. The solution for such problems can be the development of suitable lightweight, tailored material with desired properties for high-temperature applications [4]. In this regard, the idea is to develop a composite material of lightweight alloys such as aluminum and magnesium alloys which can sustain both heating and cooling environments.

Metal matrix composites (MMCs) have gained popularity in automobile industries, as few engine components are now being developed with an aluminum-alloy matrix which is reinforced with carbon fibers. Aerospace industries drew interest in MMCs reinforced with boron and graphite fibers for heating applications [2–4]. For the development of MMCs, aluminum 7075 matrix alloys are widely used in industrial applications [3]. Al7075 has proven a better alternative for heavy weighted material in the automobile and aerospace industries for its high strength-to-weight ratio with excellent mechanical and tribological properties [5, 6]. Several studies evaluate the influence of ceramic reinforcement particles, viz., SiC, B₄C, graphite, and Si₃N₄, on the mechanical, tribological, corrosion, and wear behavior of aluminum alloy-based composite [7, 8]. However, developing such MMCs with ceramic reinforcements is subject to carbon emission, which is injurious to health. The current research trend utilizes bio-waste such as chicken eggshells, fish scalps, and jute fiber as a suitable alternative reinforcement option because its properties are similar to ceramic reinforcements. Chicken eggshell is a waste and is dumped in general. Many studies proved that the application of eggshell powders, in addition to increasing the mechanical properties of the composite material, also replaces the current conventional methods, which are costly and environmentally unacceptable [9]. Moreover, it is known that by using eggshell powder, waste from agricultural production is used, and by replacing current artificial methods, this powder reduces the carbon footprint [10]. Natural ways of increasing the mechanical properties of composite materials are sought. For example, the organic eggshell, in the form of calcium oxide, is harder compared to carbide particles. These excellent properties, such as low density and thermal stability, may cause problems during technological joining operations [10, 11]. For this reason, the thermal manifestations were mapped and studied during the processing of such material. Furthermore, the eggshell powder can control the heat in the material flow during the processing because it hinders the flow of electrons and phonons freely into the matrix material [11].

There are various liquid state processing which routes like stir casting, squeeze casting, and other infiltration methods that are present to produce aluminum-based MMCs, but these are associated with several defects like porosity, shrinkage, and inclusions, which can degrade the properties of the MMCs [1]. Friction stir processing (FSP) is solid-state processing that can overcome these defects and is also applicable for microstructural modification and grain refinement, which increases grain boundaries and improves mechanical properties like metal's hardness and strength [12, 13]. The mechanism of FSP is based on friction stir welding (FSW) developed by The Welding Institute (TWI) [13]. FSP is suitable for aluminum-based alloys due to its processing capability for severe plastic deformation. In contrast, this method is also suitable for magnesium alloys as it resolves the issue of plastic deformation because of the symmetrical hexagonal structure [14, 15]. In this method, heat is generated due to friction, as a rotating tool with a shoulder and a pin tends to move in a transverse direction with applied load. This generates heat above the recrystallization temperature of the matrix metal, leading to softening of the matrix material and plastic flow occurring [12–15]. However, the process is associated with various defects, which can be overcome with the selection of suitable process parameters for FSP [14]. Few studies have been reported on the vibrational assistant to the normal processing direction of the FSP and named friction stir vibration processing (FSVP) [12, 16]. The FSVP provides a more homogeneous distribution of reinforcement and refined grain structure compared to normal FSP with negligible defects [16]. There is much literature explaining the grain refinement methods of various composite materials.

High-temperature analysis during and after the processing is important to understand the challenges associated with it. Thermal considerations of the metal matrix composites are equally important for the electronic packaging devices and aircraft components [17, 18]. In this work, the focus has been drawn on developing surface composites for defined applications to satisfy the criteria for having improved thermal characteristics. Limited literature is available on the thermal characteristics of alloys. The temperature variation concerning time during the FSP of Al7075 alloy was reported by Chai et al. [19]. The variation of temperature was recorded from room conditions (25 °C), and the peak temperature was found in the range of 300 to 350 °C taken by three thermocouples situated at equal distances in the longitudinal direction of the FSP zone. Darras et al. [20] have also done a similar study of temperature variation. However, the peak was observed in the range of 420 to 580 °C, which is approximately 70 to 90% of the melting temperature (618 °C) of Al alloy. Oddone et al. [21] measured the thermal conductivity and CTE of the aluminum and its alloy and reported the comparative studies after adding 50% graphite content to the matrix material. Their results revealed that the addition

of graphite increases the thermal conductivity up to $350 \text{ Wm}^{-1} \text{ K}^{-1}$ compared to the base material of $120 \text{ Wm}^{-1} \text{ K}^{-1}$ and reduces the CTE value from 25.2 to 17.5 ppm K^{-1} . The pure aluminum powder reinforced with short carbon fibers is also tested for thermal conductivity test, which is found in reduction from 129 to $120.6 \text{ Wm}^{-1} \text{ K}^{-1}$ with uncoated fiber addition and $113.8 \text{ Wm}^{-1} \text{ K}^{-1}$ with coated fiber reported by Hou et al. [22]. Ali et al. [17] tested the change in microstructural behavior due to the temperature variation during the FSP and reported the effect of temperature variation from 25 to $350 \text{ }^\circ\text{C}$ on microstructural and mechanical characteristics. Trojanová et al. [23] reported the thermal conductivity and CTE values during the three steps of the ARB process. The increasing fashion of thermal conductivity and decreasing CTE was observed in the range of 75 to $115 \text{ Wm}^{-1} \text{ K}^{-1}$ and 25 to $29 \times 10^{-6} \text{ K}^{-1}$, respectively. Srivastava et al. [11] have investigated the thermal characteristics such as thermal conductivity, CTE, differential thermal analysis (DTA), thermo-gravimetric analysis (TGA), and derivative thermo-gravimetric analysis (DTG) during the FSP of AZ31B/ESP surface composite. The results reveal the decreasing trend of thermal conductivity and CTE values at the increased percentage of ESP. Furthermore, the weight loss is obtained higher at a higher percentage of ESP into the base alloy during FSP. From archival literature, it can be concluded that little and insubstantial studies have been reported on the thermal studies and characterization of aluminum alloys, and insignificant work has been done on the thermal behavior of aluminum matrix composites. Hence, detailed thermal characterization is still needed to understand the behavior of aluminum matrix composite processed by friction stir processing (FSP) for high-temperature applications.

In the present work, the FSP technique is used to develop a surface composite of Al7075 alloy reinforced with waste eggshell powder (ESP) which is prepared by the ball-milling method. Temperature variation w.r.t time and peak temperature were recorded through the thermal camera and three K-type thermocouples equipped with the base plate at three equal distances. Light microscopy, FESEM images, and EBSD analysis are explored in a comparative way to validate the development of surface composite Al7075/ (3 to 9%) ESP. Furthermore, the developed samples are studied for thermal properties like thermal conductivity, CTE values, DTA, TGA, and DTG to understand the FSPed Al7075/ESP surface composite for high-temperature applications.

2 Experimental procedure

A vertical CNC milling center (made AMS) with an in-house made fixture was used in experiments. A high-speed steel tool is used in this work. The specification of the tool and other process parameters of the FSP is given in Table 1.

Table 1 Tool specifications and process parameters

Process parameters	Values
Pin profile of the tool	Pentagonal
Pin length (mm)	4
Shoulder diameter (mm)	20
Pin edges (mm)	4
Rotational speed (rpm)	3000
Tool tilt angle ($^\circ$)	0
Transverse speed (mm/min)	25

Figure 1a shows the schematic arrangement of the FSP mechanism used in the study. To measure the temperature variation over time, the base plate was equipped with a K-type thermocouple at three different locations (from the backside at a 2 mm distance from tool position during FSP stirring) along the forward direction of the FSP tool motion as shown in Fig. 1a. The present work uses a rectangular plate of Al7075 alloy of $125 \times 50 \times 6 \text{ mm}$ as a base plate. A slot of 2 mm depth and 3 mm width is made along the length of the plate to accommodate the reinforcement into it (Fig. 1b). The chemical composition of Al7075 alloy (verified at Spectro Analytical Lab Noida, India) is given in Table 2.

The ball-milled and carbonized ESP was utilized as a reinforcement. The eggshell waste was completely washed with clean water and then dried at atmospheric temperature to remove any organic layer on the surface. The ESP is first prepared with the help of ball-milling operation performed by the planetary mono mill, made by Fritsch (Pulverisette 6 classic). The specifications of ball-milling operation were kept constant such as BPR 10:1, 250 rpm, TiC ball of diameter 20 mm, and time up to 40 h. The carbonization of the ball-milled ESP was done at 500 to $600 \text{ }^\circ\text{C}$ for 4 to 5 h. The particle size of ESP was found to be in the range of 15 to $100 \text{ }\mu\text{m}$. Figure 1c and d show the ball-milled ESP and SEM image of ESP. A capping operation was performed before the FSP operation over the ESP-filled slot to encapsulate the material in the plate and close the top of the slot via surface deformation. This successfully prohibited the scattering of the reinforcement from the Al7075 plate and maintained the weight fraction of the reinforcing particles in the base plate (Fig. 1b).

Al7075/ESP samples were developed at three different proportions of ESP varying from 3 to 9% by weight. The selection range of ESP is based on the previously published literature by authors and pilot experiments. However, 10% ESP was also used to complete the experiments, but due to the limitation of slot taken on the base plate and tool pin selection accordingly, too much plowing of ESP occurred from the slot of the Al7075 alloy during FSP operation. FSP was also performed on the base plate directly without any

Fig. 1 **a** Isometric view of FSP operation and positioning of K-type thermocouple equipped with Al7075 plate, **b** ball-milled carbonized ESP used in the slot of Al7075 alloy as a reinforcement, **c** ball-milled ESP, and **d** SEM image of ESP

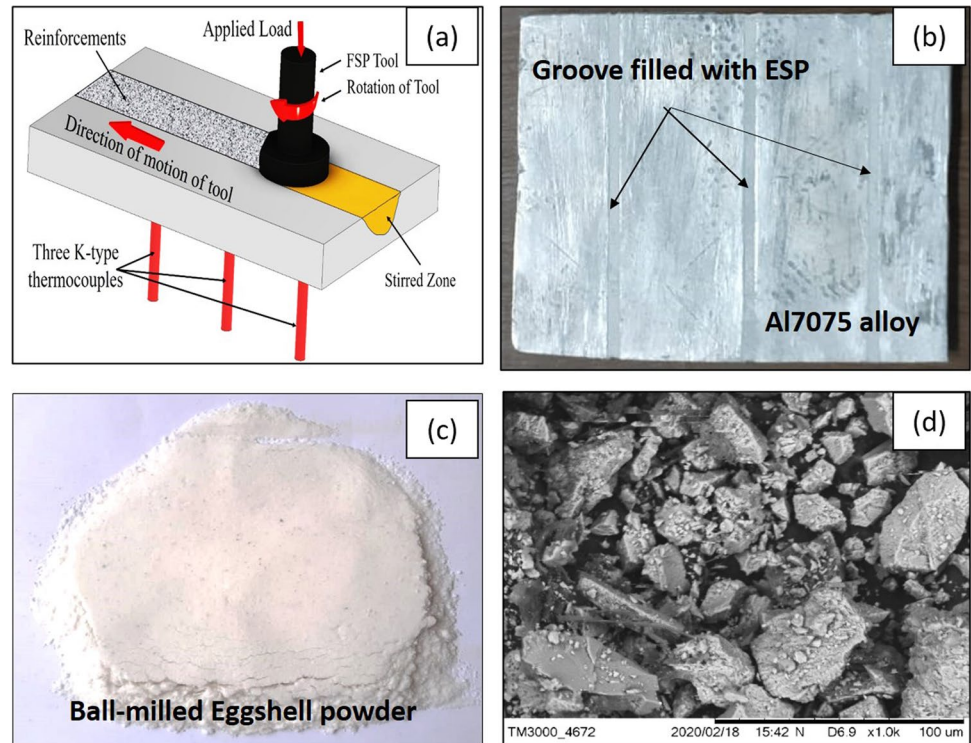


Table 2 Chemical composition of Al7075 Alloy [24, 25]

Element	Al	Mg	Zn	Mn	Si	Cu	Cr	Fe	Ti
%	91.3	1.9	3.25	0.4	0.5	1.8	0.2	0.5	0.15

Table 3 Designation and weight % of samples

S. no	Sample name	Weight % of Al7075	Weight % of ESP
1	Al7075 alloy	100	0
2	Al7075 + 3% ESP	97	3
3	Al7075 + 6% ESP	94	6
4	Al7075 + 9% ESP	91	9

reinforcement to compare the microstructural and thermal properties with reinforced samples. Table 3 shows the designation of four different samples for FSP operation.

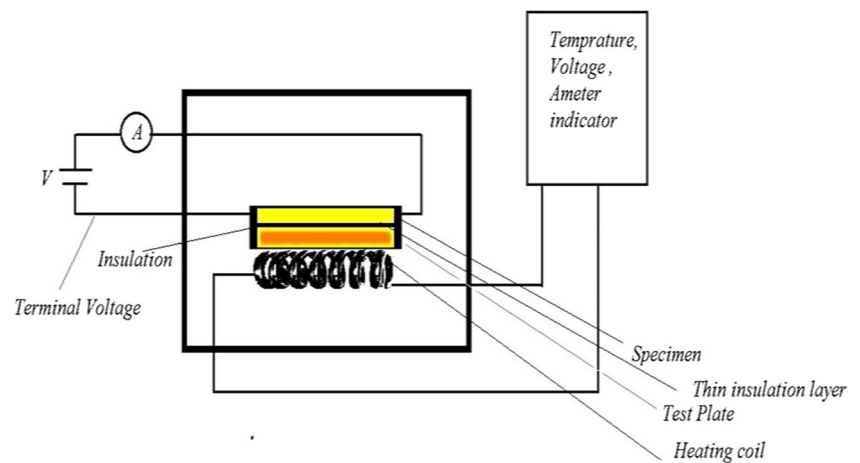
In addition to the temperature distribution analysis by K-type thermocouples, it was also confirmed by a thermal imaging camera showing the peak temperature and temperature pattern. The metallographic preparation as per ASTM E3 standard was done to validate the developed specimens to examine the microstructural measurements. The specimens were first polished with different size grit papers, followed by velvet polishing. Furthermore, Keller's reagent (15 ml HCL + 25 ml HNO₃ + 10 ml HF + 50 ml H₂O) was applied as an etchant to remove

oxide layers. The specimens were further electro-polished with 30% nitric acid and methanol solution for approximately 60 s at 15 V to conduct the morphological examination and grain size distribution study through the field emission scanning electron (FESEM) microscope (made Carl Zeiss-SIGMA), equipped with an EBSD camera. The elemental confirmation was done through EDS phase mapping images linked with FESEM.

To examine the thermal properties of the developed specimens, thermal conductivity (TC) and coefficient of thermal expansion (CTE) were evaluated through laboratory experiments. In addition to it, the thermal degradation characteristics are also conducted through the differential thermal analyzer. To check the TC of the developed FSP samples, each specimen of size (15 × 10 × 5) mm is made to place over the test plate in the modified laboratory apparatus of heat conductivity (made by K.C. Engineers Ltd). The block diagram of the heat conductivity arrangement is shown in Fig. 2.

The complete arrangement of the specimen and test plate was covered with insulation to protect them from lateral heat transfer. Thin electrical insulation was provided between the specimen and the test plate. An external voltage was also supplied to the specimen to check the effect of external voltage. The calculation of TC is based on one dimensional

Fig. 2 Block diagram of the thermal conductivity experimental arrangement



Fourier law equation. TC was measured at the temperature variation between 50 and 400 °C with a step size of 70 °C and the variation of the terminal voltage of range 100 V to 250 V with a step size of 50 V. The voltage variation was examined at an interval of 15 min with a maximum of up to 90 min. During the voltage variation, the temperature was kept constant at 330 °C. RTD sensors were used at three different locations on the test plate to measure the temperature at desired time and temperature. The CTE values are evaluated through a test specimen of size 25 mm long and 5 mm diameter by dilatometer (make NETZSCH, model DIL402E). CTE values (expansion and contraction) were recorded relative to temperature for heating and cooling in the temperature range of 50 to 400 °C. The other parameters, like heating and cooling rate, were fixed to 10 K/min in the argon atmosphere. Furthermore, a differential thermal analyzer of make EXSTAR was used to analyze the DTA, TGA, and DTG curves and the endothermic, exothermic nature, and degradation characteristics of each developed FSP sample. The range of temperature was fixed from 25 to 900 °C. The other parameters are kept constant such as a heating rate of 100 C/min, air supply of 200 ml/min, and medium nitrogen.

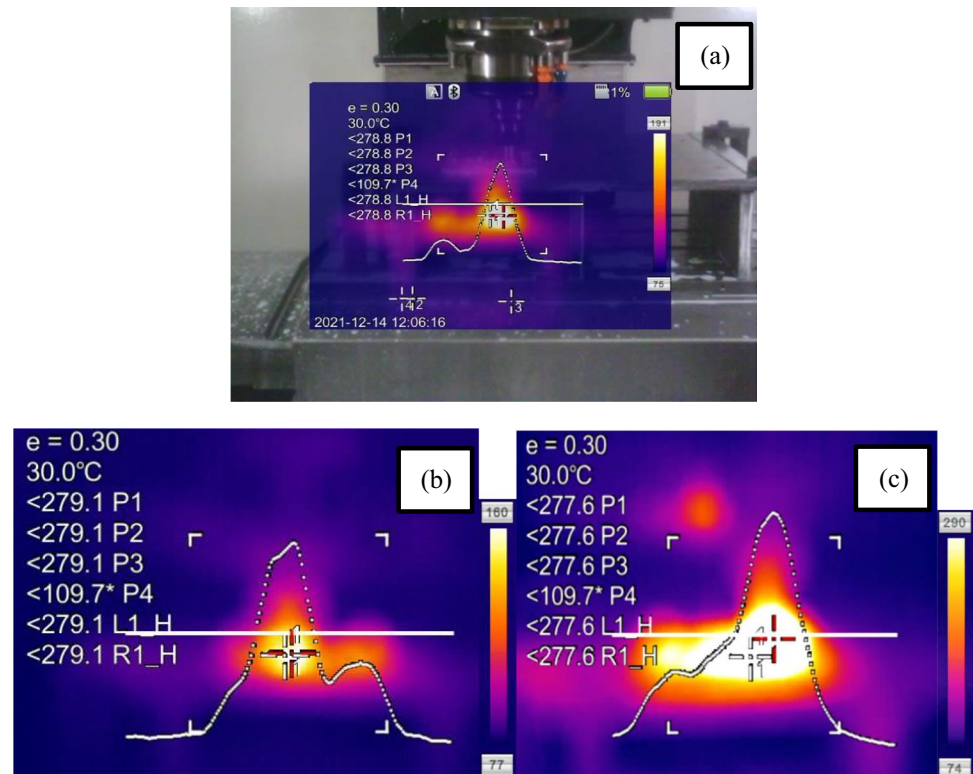
3 Results and discussion

FSP is a complicated process due to severe plastic deformation owing to the flow of material in complicated patterns. Therefore, a detailed study of the thermal behavior of the FSP is required. Infrared thermography was conducted in this study to analyze the rise in temperature by friction heating with mixing conditions. Figure 3a to c show the thermal images of each developed sample. The temperature curve shows the temperature variation at a different base plate portion. It seems that the peak temperature is observed in the stirring zone at the contact surface between the tool pin and

the top surface of the plate. During FSP, the temperature of the interface points is not constant because the tool moves in the transverse direction. As the tool moves forward, the temperature goes down. Therefore, a wave-like temperature curve is found. The ambient temperature taken was 30 °C, and the temperature reached the highest at the stirring zone was 350 °C approximately. This study is important to understand the temperature distribution along with the specimen. The temperature rise is always below the melting point of the base alloy. However, the temperature rise is high enough to change the materialistic properties, like a change in the phase of the material. This is also beneficial to find out the cause of the defect if it occurred. Similar temperature peaks and patterns were reported by previous authors also [11, 12, 19].

Furthermore, the three equipped K-type thermocouples recorded the temperature variation concerning time during each FSP run. Figure 4a shows three K-type thermocouples' locations and approximate ranges. Figure 4b to e show the graph of temperature concerning time recorded by the thermocouples for each developed sample. It has been observed from the graphs that the processing temperature varies in the range of 50 to 325 °C for all types of specimens, which confirms that the matrix alloy was not melted during the FSP. A similar range of temperature was also reported by other researchers [17]. Initially, friction increases the plastic deformation and heat generation, which rises up to a peak value due to the thermal conductive behavior of the material before passing the FSP tool along the longitudinal path. Therefore, each curve has a peak value at the nearest distance of the thermocouple with the FSP tool pin [15]. Concerning the tool movement, each run has a higher temperature on the advancing side rather than the retreating side due to the reduced thermal resistance of the unprocessed region compared to the processed region with a reduced size of grain boundary [26], which can also have confirmed by EBSD analysis (Figs. 8, 9, and 10). The peak temperature of

Fig. 3 Thermal images during FSP of **a** Al7075/3% ESP, **b** Al7075/6% ESP, **c** Al7075/9% ESP



316.9 °C was recorded by the third thermocouple for Al7075 alloy without any reinforcement, which is about 50% of the melting temperature (618 °C) of the unprocessed Al7075 alloy. It is attributed to the fact that during the FSP process, the potential energy of the electron and phonon is converted into kinetic energy due to the dislocation of atoms from their original position [11]. The grain refinement during the FSP increases the number of grain boundaries compared to the unprocessed alloy.

It restricted the transportation of the electrons and phonons from the depth of the stir zone to the top surface, leading to the lattice dislocation and reducing the peak temperature compared to the unprocessed alloy melting temperature [11, 21]. It was also found that the addition of reinforcement (ESP) and its further increment from 3 to 9% reduces the temperature range and peak temperature compared to the processed base alloy Al7075. It is owed to the fact that during the FSP, the addition of ESP hinders the grain growth at the time of softening of the base alloy, reducing the grain size more largely. It leads to a larger number of grain boundaries, which causes the lattice dislocation and scattering, reducing the temperature [18]. Another reason behind the reduced temperature range was due to the presence of an oxide layer [27]. In this study, compounds like Al₄C₃, Al₂Ca, and CaO are developed due to the interfacial reaction of Al7075 and ESP during the FSP process, creating a predominant insulating layer between the tool pin and metal surface and reducing the plastic deformation, causing

an overall reduction in temperature. An increase in hardness with increasing the percentage contribution of ESP may also be the reason for the overall reduction in temperature range [22, 27]. Figure 5a to d show the light microscopy images of the FSPed Al7075/3%ESP specimen. Distinct zones such as stir zone (SZ), thermo-mechanically affected zone (TMAZ), and heat-affected zone (HAZ) are observed from these micrographs. Fine equiaxed grains formed due to the severe level of plastic deformation and generation of high temperature during the FSP process in the stir zone of the FSPed region are observed. Furthermore, the micrographs observe the presence of ESP randomly distributed throughout the processed zone. The ESP has a unique importance during grain refinement through the FSP process because the presence of ESP controls the heat flow throughout the processed zone. It is attributed to the fact that the heat generated through the friction between the tool shoulder and base plate is also utilized to break the bonding strength of ESP due to its high melting temperature and high hardness, which leads to the coarse grain at a high percentage of reinforcement. The TMAZ region marked near the stir zone undergoes medium strain deformation and temperature peaks resulting in a lower magnitude of dynamic recrystallization than SZ, where a higher magnitude of dynamic recrystallization occurs. Also, due to the rotation and direction of the tool, the advancing side is subjected to higher temperatures leading to the generation of finer grains than the retreating side. It is attributed to the fact that the presence of ESP creates

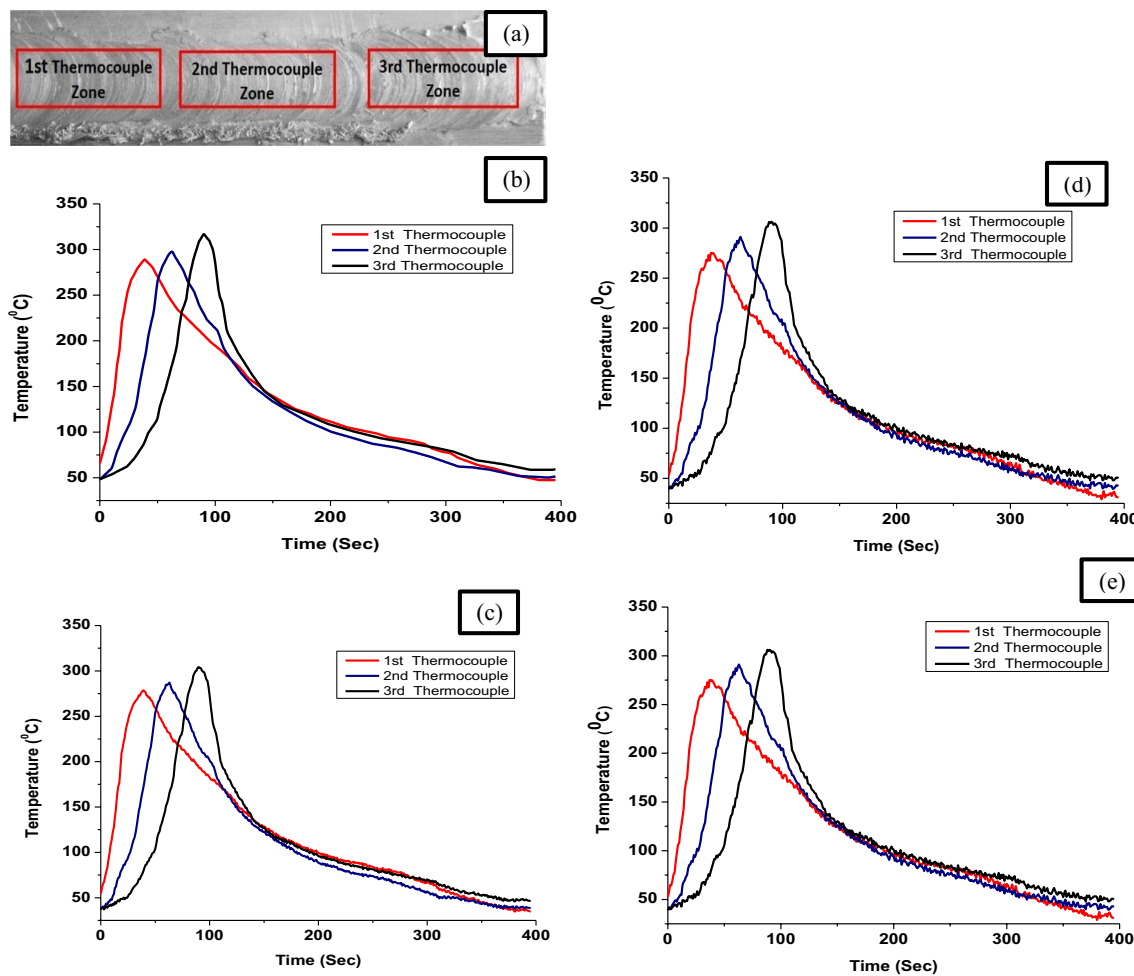


Fig. 4 a Location and approximate range of three K-type thermocouples, temperature Vs. Time response for b Al7075 FSPed alloy, c Al7075/3%ESP, d Al7075/6%ESP, e Al7075/9%ESP

a hindrance to the heat flow in the material and works like an insulating layer where ever it exists during the processing. Therefore, ESP hinders the grain growth at the time of softening of the base alloy. The heat-affected zone (HAZ) formed due to the presence of a thermal process is observed away from the center of the SZ. Larger deformation stresses and plastic deformation are not experienced in this region and show larger grain sizes. It is also known from the past literature that there is a one-to-one relationship between plastic deformation and dislocation densities [28]. Plastic deformation increases the dislocation density, resulting in a higher magnitude of dynamic recrystallization [29]. This fact also correlates to the presence of finer coaxial grain in the SZ compared to the HAZ and the advancing side of the material compared to the retreating side. Also, the higher temperature supports the stirring action of the tool for the metal flow, resulting in optimal material mixing [28–30].

Figure 6 illustrates the FESEM images of Al7075 base material after FSP (Fig. 6a), Al7075/3%ESP (Fig. 6b),

Al7075/6%ESP (Fig. 6c), and Al7075/9% ESP (Fig. 6d) from the stir zone area. In all types of specimens, it is shown that the stir zone material is adequately heated due to FSP because of friction, and severe plastic deformation is attributed to showing the occurrence of dynamically recrystallized microstructure. Layers of plasticized material move from advancing to the retreating side of the FSP tool, which presents a refined grain structure in the micrographs. The uniform distribution of the matrix material's second phase (ESP) particles indicates that the density gradient or wettability of the ESP particles and the matrix material is still excellent. The formation of a large number of uniformly dispersed ESP particles in the matrix material suggests that in situ reactions will benefit from a long-term temperature effect on the material. Thermo-mechanical effects cause a microstructural change in FSPed material [31]. It has been demonstrated that flaws such as voids or cracks are not visible in the stir zone, implying that at a rotating speed and a traverse speed of the tool, the generated heat contributes to

Fig. 5 Light microscopy images of FSPed Al7075/ESP

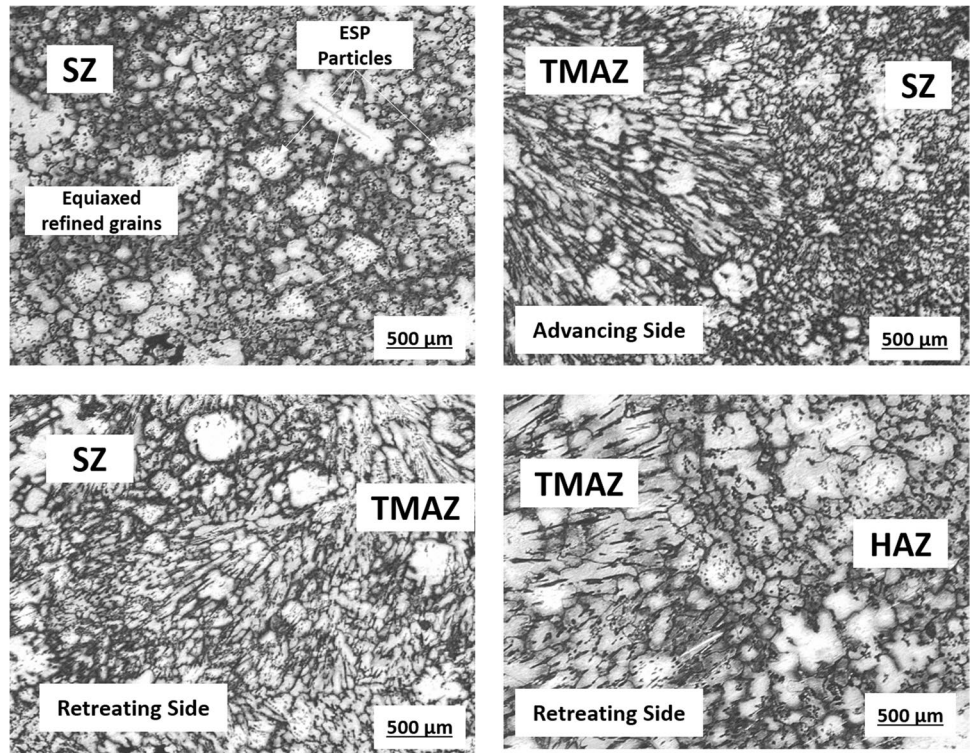
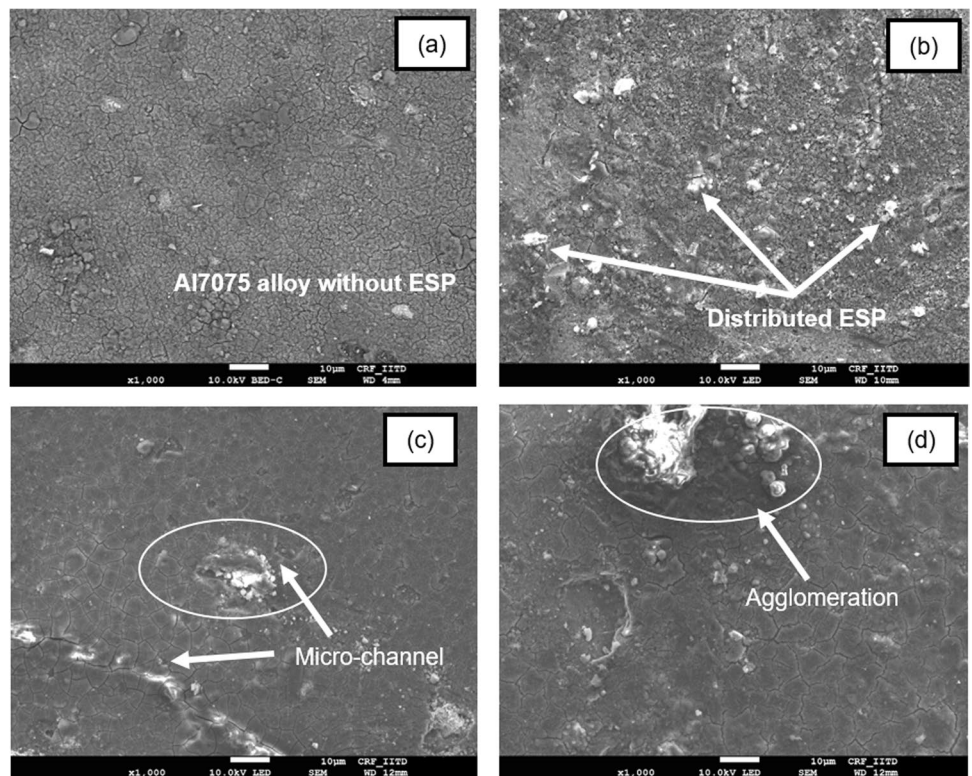


Fig. 6 FESEM images of **a** Al7075 alloy after FSP, **b** Al7075/3% ESP, **c** Al7075/6% ESP, **d** Al7075/9% ESP



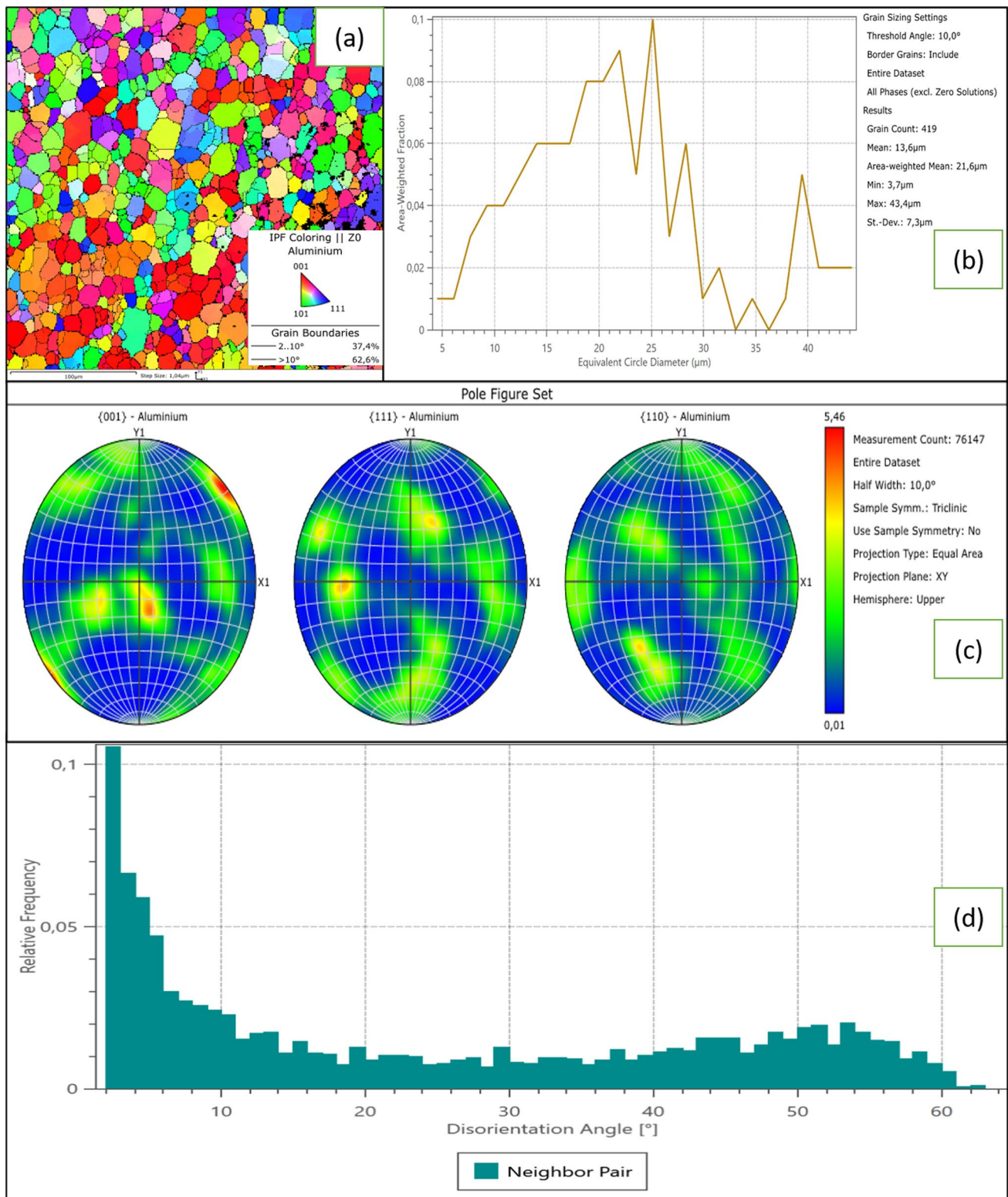


Fig. 7 FSPed Al7075 alloy without reinforcement **a** EBSD, **b** IPF, **c** grain distribution, **d** disorientation angle

grain refinement and metal strengthening [12, 15]. However, agglomeration can be seen at a higher (9%) percentage of ESP, Fig. 6d. A microchannel is also observed in Fig. 6c.

This may be due to the tunneling effect caused by the tool rotation [11]. However, FESEM has not confirmed the distribution of grains and dislocation mechanism. Therefore,

EBSD analysis of each FSPed specimen was conducted to study grain boundary, grain size, and distribution.

The EBSD image shown in Fig. 7 gives valuable inputs to trace the grain refinement in the stirred zone of FSPed Al7075 alloy without any reinforcement. In EBSD maps, grains having different crystallographic orientations have been colored differently. Larger grain sizes are observed for the FSPed sample without adding any ESP reinforcement particles. The particle grain size's average size is 13.6 μm with a deviation of 7.3 μm . Higher average grain boundaries (HAGB) having disorientation angles higher than 10° have been calculated to be 62.6% compared to lower average grain boundaries (LAGB) comprising 37.4%. The presence of a higher proportion of HAGB is attributed to the dynamic recrystallization of the grains occurring during the process, which during dynamic recovery changes the dislocation arrangement of LAGBs, resulting in the formation of boundary misorientation and, finally, the formation of HAGBs. The presence of a larger amount of HAGB also indicates the grain refinement occurring during the FSP process. This correlates with the microstructural images showing the presence of finer grains spread throughout the weld zone. According to the area-weighted mean, the average grain diameter is calculated to be 21.6 μm . Figure 8 shows the grain size distribution of the Al7075/3% ESP specimen. A larger grain size variation is observed when ESP particles are added and without particles. The mean grain size measured was 6.2 μm , and the deviation in the sizes was calculated as 2.6 μm . These refined grain sizes are due to the inclusion of new nucleation sites in the stir zone with the introduction of ESP particles. The larger region of the grain boundary contains larger stored energy which supports grain growth during the FSP process due to high-temperature deformation. However, the addition of ESP particles in the mixing area decelerates grain growth. The addition of ESP particles increases the active sites of nucleation, but the growth is reduced by pinning the grain boundaries according to the Gibb-Thomson equation [28]. Another reason for the grain refinement and formation of lower defect material is proper mixing and generation of a suitable environment. Due to the presence of these reinforced particles, increased friction occurs between the workpiece and the rotating tool. Due to this friction, the surrounding temperature increases and contributes to better flowability of the materials, and no lack of diffusion takes place [29]. This also increases the wettability of the matrix material, and the ESP-reinforced particles, increasing the elements' mutual diffusion. Therefore, mixing ESP particles increases the misorientation angles between the grains, leading to an increase in the proportion of HAGBs and improving the dynamic recrystallization process. The HAGB comprises 73.8% ($> 10^\circ$), and LAGB shares 26.2%. Figure 9 shows the grain size distribution of the Al7075/6% ESP specimen. An increase in the amount of ESP to 6%

mixed in the Al7075 alloy matrix increases the grain size of the particles in the stir zone. This increase in the dimension can be attributed to the increase in the frictional heat, which raises the temperature and results in the softening of the grains in the stir zone, leading to the clustering and agglomeration of the grains. The average grain diameter increases to an average size of 9.2 μm with a standard deviation of 5.8 μm . Also, due to the increase in the grain sizes and lowering of the dynamic recrystallization, the amount of grains with HAGBs amounts to 58.8% and LAGBs to 48.2%. Also, the majority of the grains are orientated towards 101 and 111 crystallographic planes. Figure 10 shows the grain size distribution of the Al7075/9% ESP specimen. Further addition of ESP resulted in further larger grain sizes with an average size of 10.3 μm and a deviation of 7.3 μm . Therefore, it can be easily observed the importance of the amount of reinforcement addition and its effect on the microstructure of the fabricated material. Also, this affects the dynamic recrystallization process occurring during the FSP process and the properties of the FSPed samples. The amount of HAGBs summed up 61.8% showing a misorientation angle of $> 10^\circ$, and LAGBs 38.2%, with a misorientation angle of $< 10^\circ$. The EBSD analysis proved the grains' refinement during the FSP process. Also, it showed the reason for the increased functional properties of the fabricated material having ESP as reinforced material in the Al7075 alloy matrix in optimal quantity.

3.1 Thermal conductivity

The thermal conductivity of the stirred zone is examined with an increasing percentage (3–6–9%) of ESP in the stirred zone, as shown in Fig. 11. The recorded thermal conductivity during heating was as follows: Al7075 (97–69 W/mK), Al7075 +3% ESP (87–58 W/mK), Al7075 + 6% ESP (78–55 W/mK), and Al7075 + 9% ESP (73–53 W/mK). It is observed that, with an increased temperature from 50 to 450 $^\circ\text{C}$, there is a significant decrease in thermal conductivity. It is attributed to the fact that FSP increases the number of grain boundaries and refines the grains due to severe plastic deformation. The larger number of grain boundaries interrupts the free movement of electrons and phonons, decreasing the thermal conductivity [18]. Furthermore, with an increase in ESP concentration, a decreasing trend in thermal conductivity is observed. This reflects that there is less excitation of electrons and phonons at high temperatures and high ESP concentration in the stirring region due to different energy levels of electrons and phonons of Al7075 alloy and ESP [11].

Furthermore, all the specimens were evaluated by varying the externally supplied voltage (terminal voltage) from 100 to 250 V. This was done to examine thermal conductivity concerning time through a heating coil which was

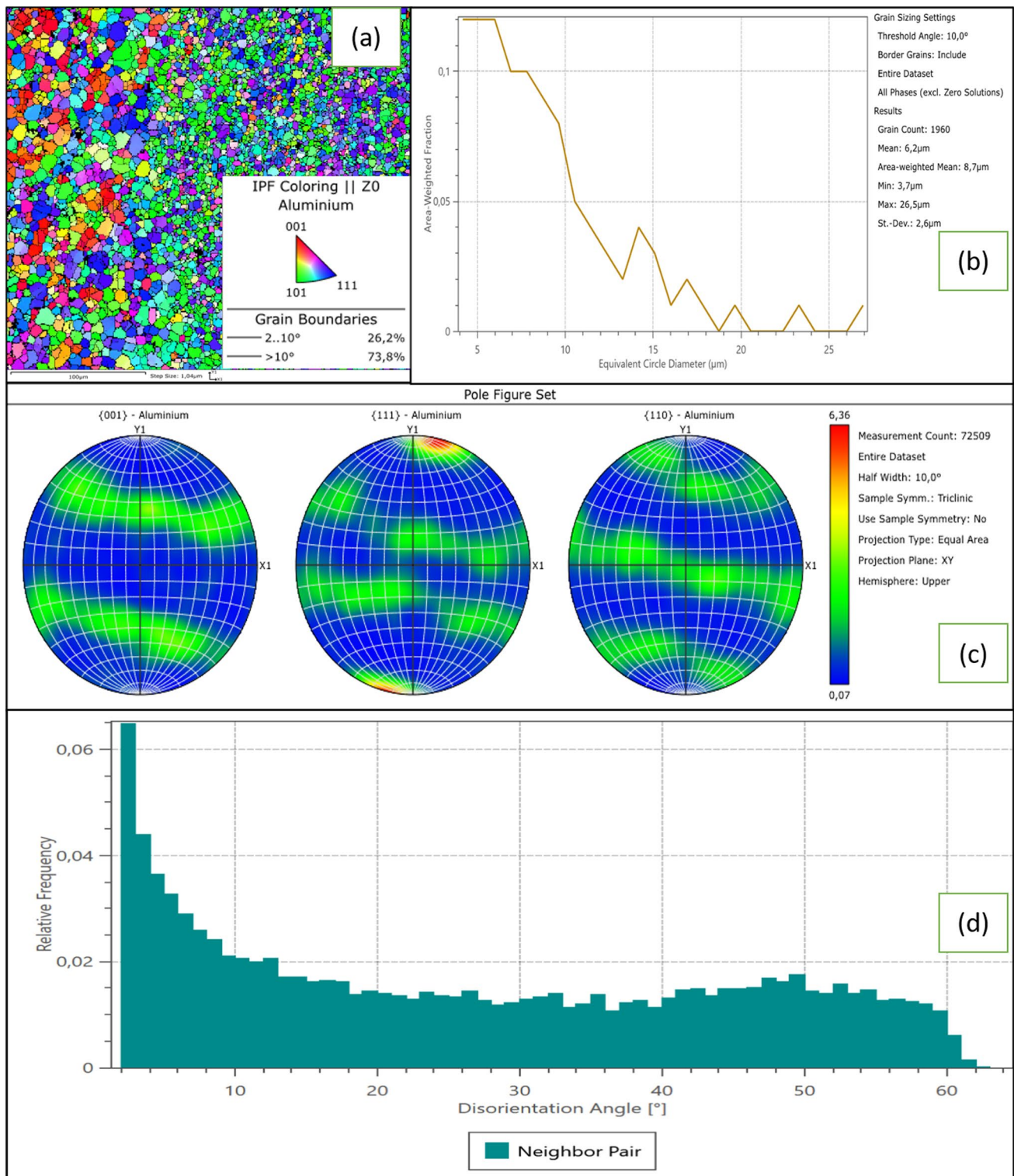


Fig. 8 FSPed Al7075/3% ESP **a** EBSD, **b** IPF, **c** grain distribution, **d** disorientation angle

fixed at 330 °C. The graphs shown in Fig. 12 reveal that the thermal conductivity increases by increasing the terminal voltage. The thermal conductivity was recorded at a

15-min time interval. With a higher supplied voltage at 250 V, the observed thermal conductivity was higher (112 W/ mK), whereas with a lower supplied voltage at 100 V, the

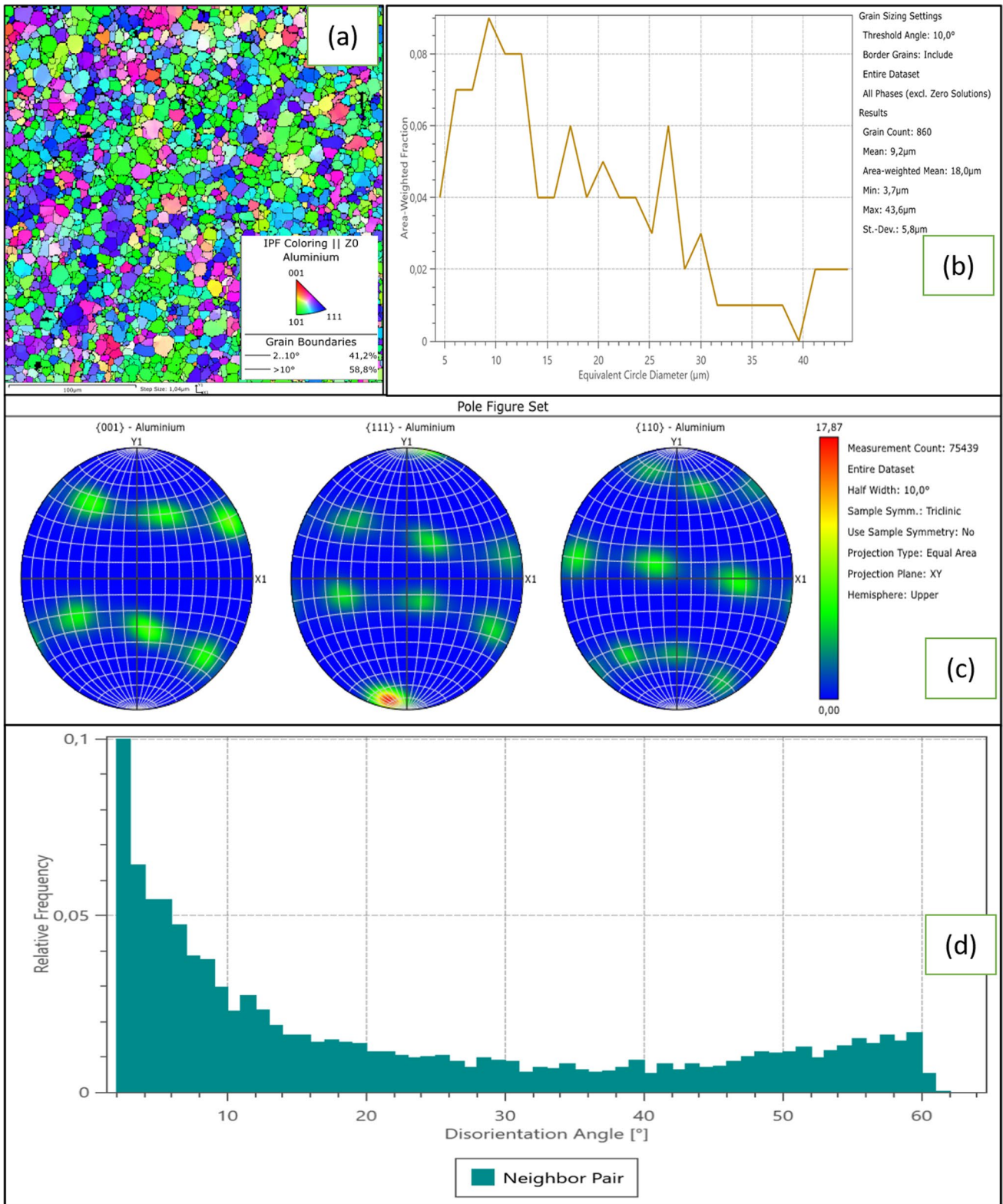


Fig. 9 FSPed Al7075/6% ESP a EBSD, b IPF, c grain distribution

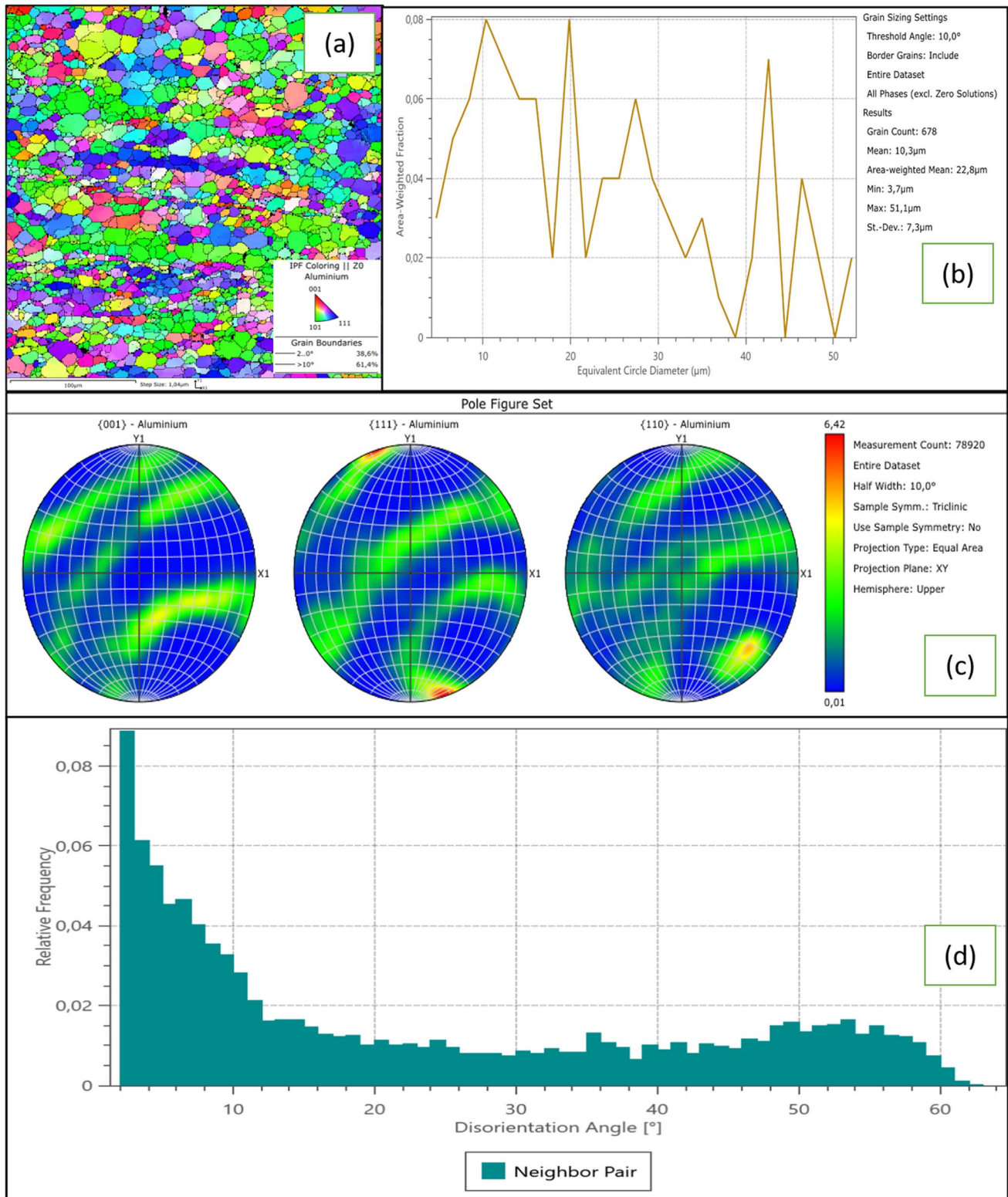


Fig. 10 FSPed Al7075/9% ESP a EBSD, b IPF, c grain distribution

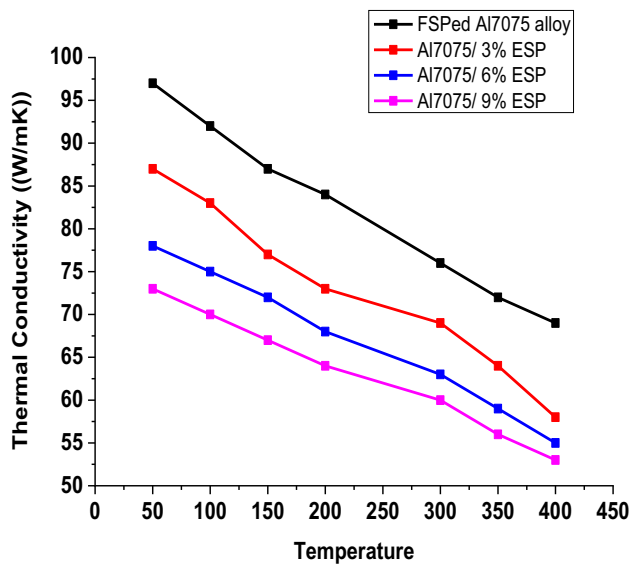


Fig. 11 Thermal conductivity vs. temperature of Al7075/ESP surface composite

observed thermal conductivity was lower (69 W/mK) for the base Al7075 alloy. While increasing the time interval, the thermal conductivity of all types of specimens decreases. Thermal conductivity at 250 V with varying ESP concentration (Al7075 +(3–9%) ESP) falls from 108 to 62 W/mK, and a similar trend is observed with lower terminal voltages as shown in Fig. 11b to d. This reveals that the thermal conductivity decreases by increasing the percentage of ESP. This is because increasing the percentage contribution of ESP into the base material develops the substantial interfacial hindrance of compounds like Al_4C_3 and Al_2Ca , which interrupt the free movement of electrons and phonons at higher terminal voltage [12–15]. Figure 11 also reveals the decreasing trend of thermal conductivity concerning time due to the decrease in time to reach the threshold temperature of 350 °C.

The CTE values were recorded through a dilatometer. Heating and cooling cycles were run from 50 to 400 °C and vice versa for each specimen of FSP along with FSPed Al7075 alloy. CTE values and their trend were recorded relative to temperature for heating and cooling as shown in Fig. 13. It is observed that, during a heating cycle, the CTE value increases logarithmically till the temperature reaches 250 °C for each specimen and declines with

Fig. 12 Thermal conductivity vs. Time with terminal voltages as a 100 V, b 150 V, c 200 V, and d 250 V

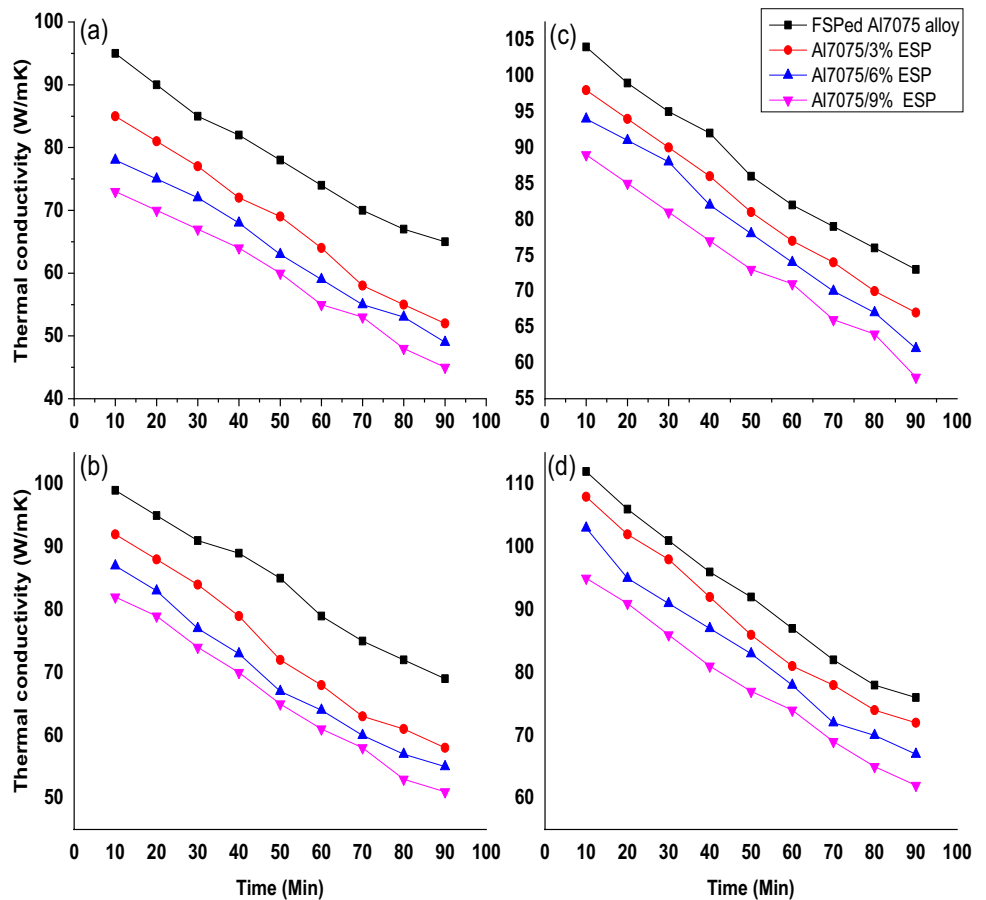
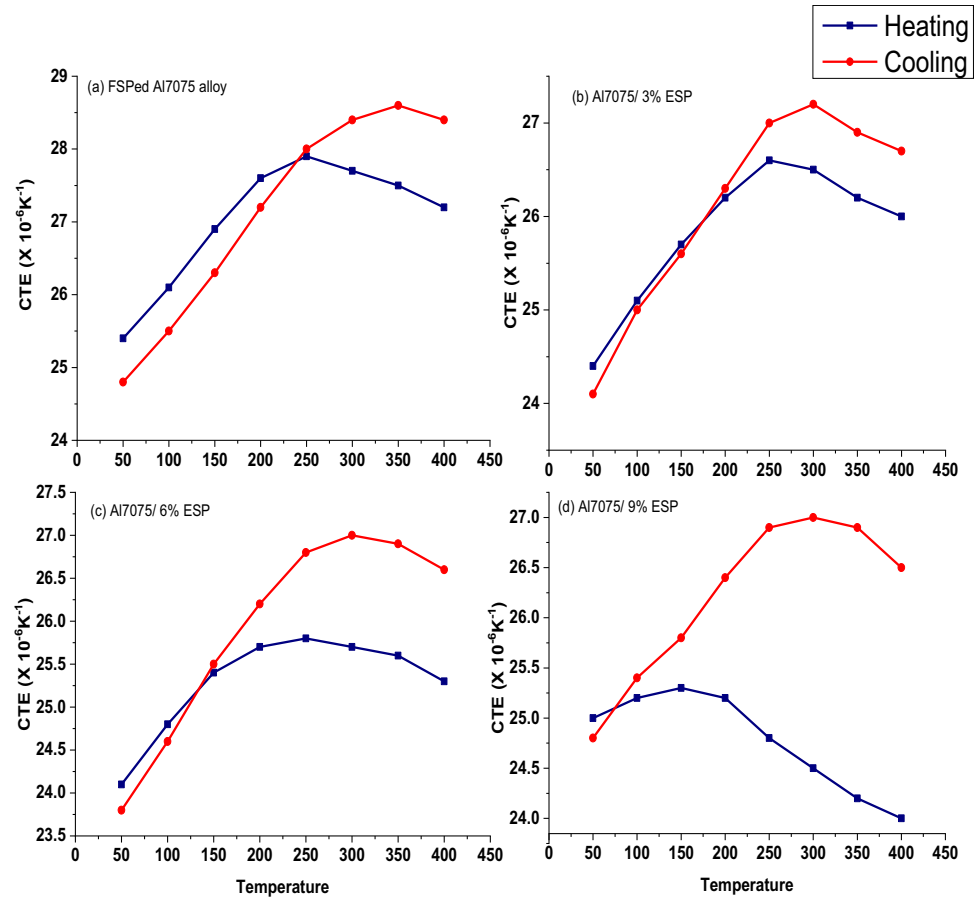


Fig. 13 CTE vs. temperature of **a** FSPed Al7075 alloy, **b** Al7075 + 3% ESP, **c** Al7075 + 6% ESP, and **d** Al7075 + 9% ESP

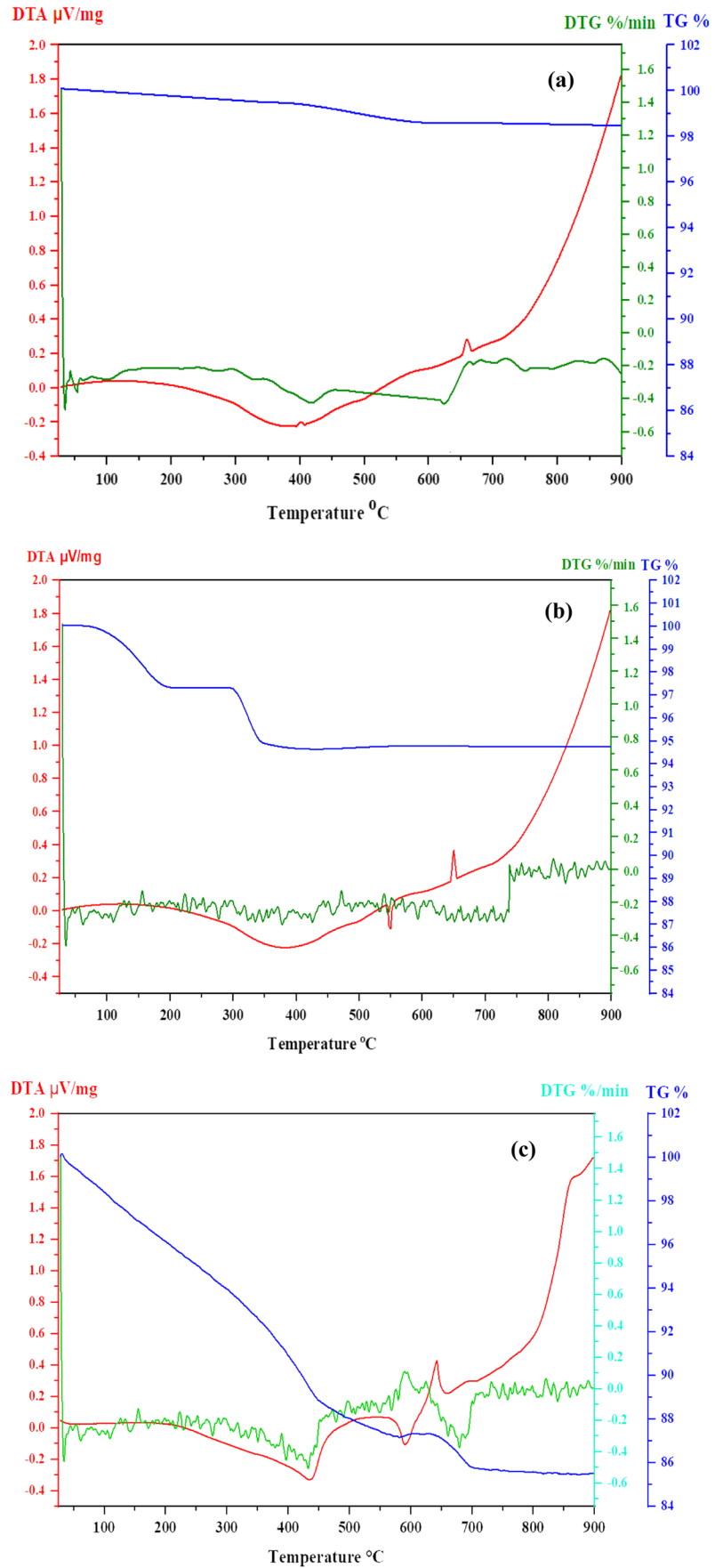


a further temperature rise. In the heating cycle, the CTE value after FSP of the base alloy increases to a maximum at 250 $^{\circ}\text{C}$ (25.4 to $27.9 \times 10^{-6} \text{ K}^{-1}$) and then starts declining up to 400 $^{\circ}\text{C}$ ($27.2 \times 10^{-6} \text{ K}^{-1}$). The recorded values for Al7075 + 3% ESP vary from 24.4 to $26.6 \times 10^{-6} \text{ K}^{-1}$ up to temperature 250 $^{\circ}\text{C}$ and further decline to $26 \times 10^{-6} \text{ K}^{-1}$ while temperature increases from 250 to 400 $^{\circ}\text{C}$ as shown in Fig. 13b. Whereas a similar trend is observed with Al7075 + 6% ESP, where the maximum value of CTE increases till the temperature reaches 250 $^{\circ}\text{C}$ and is found in the range of 24.1 to $25.8 \times 10^{-6} \text{ K}^{-1}$ and declines with a further rise in temperature upto $25.3 \times 10^{-6} \text{ K}^{-1}$ as shown in Fig. 13c. A dissimilar trend is observed with Al7075 + 9% ESP, the maximum CTE value of range 25 to $25.3 \times 10^{-6} \text{ K}^{-1}$ retrieved at 150 $^{\circ}\text{C}$ temperature (Fig. 13d). Furthermore, as temperature increases, the CTE value starts decreasing up to $24 \times 10^{-6} \text{ K}^{-1}$ at 400 $^{\circ}\text{C}$. CTE value is higher in all the cooling cycle compared to the heating cycle, as shown in Fig. 13a to d. The ESP-reinforced specimen’s CTE values are lower than that of Al7075 alloy. In the cooling cycle, the maximum CTE value of Al7075 alloy after FSP is at 350 $^{\circ}\text{C}$ ($28.6 \times 10^{-6} \text{ K}^{-1}$). The maximum CTE of surface composite Al7075/ESP is obtained at 300 $^{\circ}\text{C}$ for Al7075 + 3% ESP as $27.2 \times 10^{-6} \text{ K}^{-1}$ and minimum at 50 $^{\circ}\text{C}$ for Al7075 + 6% ESP as 23.8

$\times 10^{-6} \text{ K}^{-1}$. It is because FSPed specimens have refined and equiaxed grain and a large number of grain boundaries. While increasing the temperature, the CTE values increase until the recrystallization starts, which is approximately in the range of 250 to 330 $^{\circ}\text{C}$ [30, 32]. Once the recrystallization starts, the thermal stresses are increased and act as a thermal barrier for the free motion of electrons and phonons, leading to a decrease in CTE values [21, 33]. While during the cooling cycle, thermal stresses are reduced due to temperature drop and contraction. Hence, a logarithmic relation is maintained for the CTE values [30]. Furthermore, increasing the ESP percentage, CTE values decrease due to an increase in thermal stress arising due to a mismatch of CTE values of Al7075 alloy and ESP.

DTA, DTG, and DTG of the FSPed sample were tested for Al7075 + 3% ESP, Al7075 + 6% ESP, and Al7075 + 9% ESP shown in Fig. 14a to c. It can be observed from Fig. 14a that the mass of the compound was 100% at 27 $^{\circ}\text{C}$ at the beginning of the process. The maximum temperature was 900 $^{\circ}\text{C}$ in all the cases. With the rise in temperature of 360 $^{\circ}\text{C}$, there is a weight loss of 0.4%. A rapid loss in weight is observed when the temperature starts elevating from 423 $^{\circ}\text{C}$, the TG% curve becomes steeper, and the maximum weight loss increases by 1.53%. The DTA curve representing exothermic

Fig. 14 DTA, TGA, and DTG curve for **a** Al7075+3% ESP, **b** Al7075+6% ESP, and **c** Al7075+9% ESP



reaction shows peaks at 397.4 °C and 659.7 °C. The DTA curve tends to increase smoothly with a further temperature rise and represents an exothermic peak at 900 °C, where the weight loss is maximum. The decomposition curve of DTG becomes stable when the temperature rises from 138 °C and continues to 245 °C. Furthermore, an increase in temperature results in a fall in decomposition percentage by 0.38% at 420 °C. The second stage of decomposition is observed with a peak at 686.5 °C. A similar pattern is observed for 6% and 9% ESP specimens (shown in Fig. 14b–c), where the weight loss is observed at 5.25% at 575.6 °C and 14.62% at 830.8 °C. Similar findings were also reported by previous authors [11, 34]. Since the matrix is reinforced with ESP, weight loss is attributed to an increase in the percentage of ESP, which contains the moisture and impurity to be burned. Another reason behind the weight loss is the increasing hindrance in the motion of photons and free electrons while increasing the ESP percentage, which is also responsible for oxide layer formation at the parent material. These oxide layers are later broken with an increase in temperature above the recrystallization temperature, which also changes the enthalpy of the matrix material. Some impurities are burnt at high temperatures, which reflects sudden weight losses, which are also represented by a change in enthalpy [34]. On examination of thermal degradation, several exothermic peaks in the DTA curve are found with composite at changing the percentage of ESP. The release of heat during this process results in a positive temperature difference.

4 Conclusion

A surface composite is developed with Al7075 and 3–9% varying reinforcement of eggshell powder by friction stir processing. The outcome shows that:

- (1) The temperature profile and readings of the K-type thermocouple illustrate the peak temperature in the range of 300 to 350 °C.
- (2) The randomly dispersed eggshell powder is seen in the micrographs. The fine equiaxed, refined grains with a large number of grain boundary is observed in the different zones of the FSP subject to dynamic recrystallization and grain recovery.
- (3) FESEM images show the defect-free surface composite with a negligible amount of agglomeration. It has been demonstrated that flaws such as voids or cracks are not visible in the stir zone, implying that at a rotating speed and a traverse speed of the tool, the generated heat contributes to grain refinement and metal strengthening.
- (4) EBSD analysis confirms the presence of both continuous and discontinuous types of grains in the stir zone,

and it increases with the increased percentage of eggshell powder. The minimum grain size is measured to be 6.2 to 10.3 μm at the varying percentage of eggshell powder (3 to 9%) in the stir zone, respectively.

- (5) The thermography result revealed the decreasing trend of thermal conductivity, and CTE and the values were found in the range of 97 to 53 W/mK, and 26.6 to $24 \times 10^{-6} \text{ K}^{-1}$ (heating cycle), 27.2 to $23.8 \times 10^{-6} \text{ K}^{-1}$ (cooling cycle), respectively at an increasing ESP percentage.
- (6) The highest and lowest thermal conductivity of 108 W/mK and 62 W/mK was observed at higher and lower terminal voltages of 250 V and 100 V, respectively, at 15-min time intervals.
- (7) The DTA, TGA, and DTG curves explored that the maximum weight loss varies up to 5.25% with exothermic peaks and decomposition steps for each surface composite.

Author contribution Conceptualization, Ashish Kumar Srivastava; methodology, Ashish Kumar Srivastava and Suryank Dwivedi; software, Akash Nag, and Suryank Dwivedi; validation, Amit Rai Dixit and Sergej Hloch; formal analysis, Ashish Kumar Srivastava, Akash Nag, and Suryank Dwivedi; investigation, Ashish Kumar Srivastava and Suryank Dwivedi; Resources, Amit Rai Dixit and Sergej Hloch; data curation, Ashish Kumar Srivastava, Akash Nag, and Suryank Dwivedi; writing—original draft preparation, Ashish Kumar Srivastava, Akash Nag, and Suryank Dwivedi; writing—review & editing, Akash Nag, Suryank Dwivedi, Amit Rai Dixit, and Sergej Hloch; visualization, Ashish Kumar Srivastava, Supervision, Amit Rai Dixit, and Sergej Hloch.

Funding Open access funding provided by The Ministry of Education, Science, Research and Sport of the Slovak Republic in cooperation with Centre for Scientific and Technical Information of the Slovak Republic

Declarations

Ethics approval The research does not involve human participants or animals, and the authors warrant that the paper fulfils the ethical standards of the journal.

Consent to participate It is confirmed that all the authors are aware and satisfied with the authorship order and correspondence of the paper.

Consent for publication All the authors are satisfied that the last revised version of the paper is published without any changes.

Competing interests The authors declare no competing interests.

Open Access This article is licensed under a Creative Commons Attribution 4.0 International License, which permits use, sharing, adaptation, distribution and reproduction in any medium or format, as long as you give appropriate credit to the original author(s) and the source, provide a link to the Creative Commons licence, and indicate if changes were made. The images or other third party material in this article are

included in the article's Creative Commons licence, unless indicated otherwise in a credit line to the material. If material is not included in the article's Creative Commons licence and your intended use is not permitted by statutory regulation or exceeds the permitted use, you will need to obtain permission directly from the copyright holder. To view a copy of this licence, visit <http://creativecommons.org/licenses/by/4.0/>.

References

1. Srivastava AK, Dixit AR, Tiwari S (2016) A review on the intensification of metal matrix composites and its nonconventional machining. *Sci Eng Compos Mater* 25(2):213–228. <https://doi.org/10.1515/secm-2015-0287>
2. Srivastava AK, Gupta Y, Patel S, Tiwari SK, Pandey S (2019) Metal matrix composites—a review on synthesis and characterization. *IOP Conf Ser Mater Sci Eng* 691:012077. <https://doi.org/10.1088/1757-899X/691/1/012077>
3. Kulekci MK (2008) Aluminum and its alloys applications in automotive industry. *Int J Adv Manuf Technol* 39:851–865
4. Karpasad F, Abbasi A, Ardestani M (2020) Effect of amount of TiB₂ and B₄C particles on tribological behaviour of Al7077/TiB₂/B₄C mono and hybrid surface composites produced by friction stir processing. *Surf Coat Technol* 390:125680. <https://doi.org/10.1016/j.surfcoat.2020.125680>
5. Ibrahim IA, Mohamed FA, Lavernia EJ (1991) Particulate reinforced metal matrix composites - a review. *J Mater Sci* 26:1137–1156
6. Dey KMP (2015) Aluminum metal matrix composites—a review. *Rev Adv Mater Sci* 42:58–67
7. Lloyd DJ (1994) Particle reinforced aluminium and aluminum matrix composites. *Int Mater Rev* 39(1):1–23
8. Ye HZ, Liu XY (2004) Review of recent studies in aluminum matrix composites. *J Mater Sci* 39:6153–6171
9. Guru PS, Dash S (2014) Sorption on eggshell waste—a review on ultrastructure, biomineralization and other applications. *Adv Colloid Interf Sci* 209:49–67
10. Laca A, Laca A, Díaz M (2017) Eggshell waste as catalyst: a review. *J Environ Manage* 197:351–359
11. Srivastava AK, Saxena A, Dixit AR (2021) Investigation on the thermal behaviour of AZ31B/waste eggshell surface composites produced by friction stir processing. *Compos Commun* 28:100912. <https://doi.org/10.1016/j.coco.2021.100912>
12. Bagheri B, Abdollahzadeh A, Sharifi F, Abbasi M, Moghaddam AO (2021) Recent development in friction stir processing of aluminum alloys: Microstructure evolution, mechanical properties, wear and corrosion behaviors. *Proc Inst Mech Eng Part E J Process Mech Eng*. <https://doi.org/10.1177/09544089211058007>
13. Abdollahzadeh A, Bagheri B, Abbasi M, Sharifi F, Moghaddam AO (2021) Mechanical, wear and corrosion behaviors of AZ91/SiC composite layer fabricated by friction stir vibration processing. *Surf Topogr Metrol Prop* 9:035038. <https://doi.org/10.1088/2051-672X/ac2176>
14. Alizadeh M, Bagheri B, Shamsipur A et al (2022) A new investigation into Al-Cu dissimilar joint by SiC nanoparticle during the FSSW process: influence of rotational speed and dwell time, 17 May 2022. PREPRINT (Version 1) available at Research Square. <https://doi.org/10.21203/rs.3.rs-1640449/v1>
15. Bagheri B, Abbasi M, Abdollahzadeh A, Mirsalehi SE (2020) Effect of second-phase particle size and presence of vibration on AZ91/SiC surface composite layer produced by FSP. *Trans Nonferrous Metals Soc China* 30(4):905–916. [https://doi.org/10.1016/S1003-6326\(20\)65264-5](https://doi.org/10.1016/S1003-6326(20)65264-5)
16. Bagheri B, Abbasi M, Abdollahzadeh A et al (2020) A comparative study between friction stir processing and friction stir vibration processing to develop magnesium surface nanocomposites. *Int J Miner Metall Mater* 27:1133–1146. <https://doi.org/10.1007/s12613-020-1993-4>
17. Moghaddas MA, Kashani-Bozorg SF (2013) Effects of thermal conditions on microstructure in nanocomposite of Al/Si₃N₄ produced by friction stir processing. *Mater Sci Eng A* 559:187–193
18. Suganeswaran K, Parameshwaran R, Thangavel P, Nithyavathy N, Sivasakthivel T (2019) Investigations on micro hardness, electrical and thermal conductivity of AA7075 surface hybrid composites produced through friction stir processing. *Mater Res Express* 6:116548
19. Chai F, Zhang D, Li Y (2014) Effect of thermal history on microstructures and mechanical properties of AZ31 aluminum alloy prepared by friction stir processing. *Materials* 7:1573–1589
20. Darras BM, Omar MA, Khraisheh MK (2007) Experimental thermal analysis of friction stir processing. *Mater Sci Forum* 539-543:3801-3806 Online: 2007-03-15 (2007) Trans Tech Publications, Switzerland. <https://doi.org/10.4028/www.scientific.net/MSF.539-543.3801>
21. Oddone V, Boerner B, Reich S (2017) Composites of aluminum alloy and aluminum alloy with graphite showing low thermal expansion and high specific thermal conductivity. *Sci Technol Adv Mater* 18(1):180–186
22. Hou LG, Wu RZ, Wang XD, Zhang JH, Zhang ML, Dong AP, Sun BD (2017) Microstructure, mechanical properties and thermal conductivity of the short carbon fiber reinforced aluminum matrix composites. *J Alloy Compd*. <https://doi.org/10.1016/j.jallcom.2016.11.422>
23. Trojanová Z, Halmešová K, Drozd Zdeněk, Šíma V, Luká P, Džugan J, Minárik P (2018) Thermal conductivity of an AZ31 sheet after accumulative roll bonding. *Crystals* 8:278. <https://doi.org/10.3390/cryst8070278>
24. Dwivedi R, Singh RK, Kumar S, Srivastava AK (2021) Parametric optimization of process parameters during the friction stir processing of Al7075/SiC/waste eggshell surface composite. *Mater Today Proc*. <https://doi.org/10.1016/j.matpr.2021.03.545>
25. Dwivedi R, Singh RK, Srivastava AK, Anand A, Kumar S, Pal A (2021) Statistical optimization of process parameters during the friction stir processing of Al7075/Al₂O₃/waste eggshell surface composite. *Recent Trends in Industrial and Production Engineering. Lect Notes Mech Eng*. https://doi.org/10.1007/978-981-16-3330-0_9
26. Shen Z, Zhang M, Li D et al (2023) Microstructural characterization and mechanical properties of AlMg alloy fabricated by additive friction stir deposition. *Int J Adv Manuf Technol* 125:2733–2741. <https://doi.org/10.1007/s00170-023-10952-x>
27. Cartigueteyn S, Mahadevan K (2019) Effects of thermal conditions on microstructure and mechanical properties of Cu–SiCp surface nanocomposites by friction stir processing route. *Trans Indian Inst Met* 72:289–305
28. Bagheri B, Alizadeh M, Mirsalehi SE et al (2022) Nanoparticles Addition in AA2024 aluminum/pure copper plate: FSSW approach, microstructure evolution, texture study, and mechanical properties. *JOM* 74:4420–4433. <https://doi.org/10.1007/s11837-022-05481-z>
29. Bagheri B, Abdollahzadeh A, Shamsipur A (2023) A different attempt to analysis friction stir spot welding of AA5083-copper alloys. *Mater Sci Technol*. <https://doi.org/10.1080/02670836.2022.2159633>
30. Lunetto V, De Maddis M, Russo Spena P (2023) Similar and dissimilar lap friction stir welding of titanium alloys: on the elimination of the hook defect. *Int J Adv Manuf Technol*. <https://doi.org/10.1007/s00170-023-11316-1>

31. Bagheri B, Shamsipur A, Abdollahzadeh A et al (2023) Investigation of SiC nanoparticle size and distribution effects on microstructure and mechanical properties of Al/SiC/Cu composite during the FSSW process: experimental and simulation. *Met Mater Int* 29:1095–1112. <https://doi.org/10.1007/s12540-022-01284-8>
32. Hassan S, Aigbodion V (2015) Effects of eggshell on the microstructures and properties of Al-Cu-Mg/eggshell particulate composites. *J King Saud Univ Eng Sci* 27(1):49–56
33. Lukáè P, Rudajevová A (2003) Thermal expansion in aluminum composites. *Kov Mater* 41(5):281–292
34. Lal S, Kumar S, Khan ZA (2018) Microstructure evaluation, thermal and mechanical characterization of hybrid metal matrix composite. *Sci Eng Compos Mater* 25(6):1187–1196

Publisher's note Springer Nature remains neutral with regard to jurisdictional claims in published maps and institutional affiliations.